New physics searches in a low threshold scintillating argon bubble chamber measuring coherent elastic neutrino-nucleus scattering in reactors

E. Alfonso-Pita,[1,*] L. J. Flores,[2,†] Eduardo Peinado,[1,‡] and E. Vázquez-Jáuregui[1,§]

[1]*Instituto de Física, Universidad Nacional Autónoma de México, A.P. 20-364, Ciudad de México 01000, México*

[2]*Tecnológico Nacional de México/ITS de Jerez, C.P. 99863, Zacatecas, México*

(Received 28 March 2022; accepted 3 June 2022; published 24 June 2022)

The sensitivity to new physics of a low threshold scintillating argon bubble chamber measuring coherent elastic neutrino-nucleus scattering in reactors is reported. Namely, light scalar mediators, sterile neutrino oscillations, unitarity violation, and nonstandard interactions are studied. The results indicate that this detector could be able to set stronger constraints than current limits set by the recent COHERENT measurements. Considering the best scenario, a 100 kg detector located 30 m from a 2000 MW_{th} reactor, a sterile neutrino search would cover most of the space parameter allowed from the reactor antineutrino anomaly fit. Unitarity violation studies could set constraints on α_{11}, more stringent than the current oscillation experiments fit. A low threshold argon detector with very low backgrounds has the potential to explore new physics in different scenarios and set competitive constraints.

DOI: 10.1103/PhysRevD.105.113005

I. INTRODUCTION

Coherent elastic neutrino-nucleus scattering (CEνNS) is a Standard Model (SM) process that has attracted interest from the physics community. CEνNS offers the possibility to perform high precision measurements in several processes of the SM [1–6], as well as exploring new physics (NP) scenarios in nuclear and particle physics [7–12]. CEνNS was first observed by The COHERENT collaboration using a Cesium Iodide (CsI) [Na] crystal [13] and later with a liquid argon (LAr) detector [14] in the spallation source Spallation Neutron Source at Oak Ridge. This elusive process is still pending, to be observed for neutrinos produced in nuclear reactors, and it is currently a race among several collaborations [1,15–22]. Recently, evidence of its observation has been reported using a germanium detector [23], indicating that the first measurement of this process for reactor neutrinos is expected within less than a couple of years. The observation of this process requires a device capable to detect low-energy nuclear recoils and achieve low backgrounds operating at low energy thresholds (sub keV) for long time periods.

Several detectors are currently taking data [15,16,24] or under construction [1,18–22]. The Scintillating Bubble Chamber (SBC) collaboration is developing a low threshold argon scintillating bubble chamber aiming to achieve a 100 eV threshold. This device is insensitive to electromagnetic interactions, which greatly suppresses the majority of the backgrounds [25,26].

A study of the physics reach of the Scintillating Bubble Chamber detector showed its high sensitivity to the weak mixing angle, neutrino magnetic moment, and the search for a light Z' gauge boson mediator [26]. This work extends the physics potential of this detector to other new physics scenarios, such as searches for light scalar mediators, sterile neutrinos, unitarity violation, and nonstandard interactions. The analysis reported in this manuscript also applies to any other technique reaching 100 eV nuclear recoils, eliminating electron-recoil backgrounds, and scaling to 10–100 kg target masses.

A brief description of the experimental scenarios considered is given in the next section (Experiment Description). The following section (New Physics) describes the analysis methods to extract the sensitivity to NP.

II. EXPERIMENT DESCRIPTION

The Scintillating Bubble Chamber is a superheated detector based on 10 kg of LAr [25,26]. The detector consists of two fused silica vessels, an inner and an outer jar. The target fluid is contained between the jars, and this

*ernestoalfonso@estudiantes.fisica.unam.mx
†ljflores@jerez.tecnm.mx
‡epeinado@fisica.unam.mx
§ericvj@fisica.unam.mx

TABLE I. Relevant parameters assumed for the setups considered and expected backgrounds estimated with a GEANT4 simulation.

Setup	LAr mass (kg)	Power (MW_{th})	Distance (m)	CEνNS events per day	Anti-ν flux uncertainty (%)	Threshold uncertainty (%)	Backgrounds (events/day)					
							Reactor			Cosmogenic		Total
							Neutrons	(γ, n)	Thomson	Neutrons	(μ, n)	
A	10	1	3	8.1	2.4	5	0.003	0.22	0.0002	0.38	0.47	1.07
B	100	2000	30	1565.2	2.4	5	0	0	0	125	55	180
B(1.5)	100	2000	30	1565.2	1.5	2	0	0	0	125	55	180

system is immersed in a pressure vessel filled with liquid CF_4 acting as thermal bath and hydraulic fluid. The chamber is designed to operate with a low threshold of 100 eV. This detector has a system of 32 SiPMs [Hamamatsu vacuum ultraviolet 4 Quads); these sensors record the light created in the LAr and allow background discrimination. In addition, an array of eight piezoelectric sensors are coupled to the quartz jar to register the acoustic signal created during the bubble formation. Three cameras and lenses are located outside the pressure vessel for imaging of the bubbles produced in the LAr.

A bubble chamber has excellent characteristics for the detection of neutrinos via coherent elastic scattering with argon nuclei. This detector presents high discrimination levels for electromagnetic backgrounds and sub-keV operating threshold allowing the detection of nuclear recoils induced by CEνNS. A xenon bubble chamber has already been operated at lower thresholds than fluorocarbon-based chambers [27], currently reaching thresholds down to 500 eV.[1] This has demonstrated insensitivity to electron recoil backgrounds at the sub-keV threshold with simultaneous scintillation and bubble nucleation induced by nuclear recoils. The main challenge of this experiment is to keep stable operation conditions for long periods of time with rejection of electron recoils of the order of 10^{-8}. Sub-keV thresholds have already been reached by bubble chambers using noble liquids [28,29].

The SBC collaboration is developing a dedicated calibration program to constrain the nucleation efficiency function for different thermodynamic conditions and calibrate the detector response at a 100 eV threshold. This program includes photo-neutron sources producing nearly monoenergetic neutrons at different energies (9, 23, 94, and 380 keV) and also includes the calibration of nuclear recoils via Thomson scattering produced by MeV γ rays. The expertise to develop this program is built upon the successful calibration program developed by the PICO collaboration [30,31].

Three experimental setups are explored in this work, assuming one year of live time. Setup A assumes a 10 kg LAr chamber located 3 m from a 1 MW_{th} reactor, and setup B considers a 100 kg LAr chamber located at 30 meters from a 2000 MW_{th} power reactor. Setups A and B use 2.4% uncertainty in the antineutrino flux. Setup B(1.5) is the same as setup B but uses a 1.5% uncertainty in the antineutrino flux (this is the uncertainty measured by the Daya Bay experiment from the reactors of the Daya Bay and Ling Ao nuclear power plants) [32]. The calibration strategy for the detector and backgrounds estimated with a GEANT4 [33–35] Monte Carlo simulation used for the study described in this manuscript are described elsewhere [26]. Table I shows the main parameters assumed for the three setups considered and the expected backgrounds estimated with the GEANT4 simulation. The relevant backgrounds are divided into two main categories; reactor backgrounds, produced by neutrons, (γ, n) reactions and Thomson scattering, and cosmogenic backgrounds, produced by neutrons and spallation (μ, n) reactions.

A Training, Research, Isotopes, General Atomics Mark III research reactor located at the National Institute for Nuclear Research (ININ) near Mexico City is being explored as a possible location for setup A. This reactor is movable, located inside a water pool, that would allow baselines between 3 and 10 m. The Laguna Verde (LV) power reactor consisting of two boiling water reactors-5 units located on the east coast of Mexico in the Gulf of Mexico is also explored as a possible location for setups B.

III. NEW PHYSICS

The potential to probe NP scenarios with the 10 kg and 100 kg LAr bubble chambers in the three proposed setups is investigated. The functional form of the nucleation efficiency is described by a normal cumulative distribution function (Gaussian cumulative distribution function), following the approximated shape measured in C_3F_8 [30,31]. The probability of a recoil to nucleate a bubble is then expressed as

$$Pr(T) = \frac{1}{2}\left(1 + \mathrm{erf}\left(\frac{T - E_T}{\sigma\sqrt{2}}\right)\right), \quad (1)$$

[1]Low-threshold performance from private communication, publication in preparation by the SBC collaboration.

where T is the energy of the recoil, $E_T = 100$ eV and $\sigma = 10$ eV.

The Standard Model cross section for CEνNS is

$$\frac{d\sigma}{dT} = \frac{G_F^2}{2\pi} M_N Q_w^2 \left(2 - \frac{M_N T}{E_\nu^2}\right) F^2(q^2), \tag{2}$$

where E_ν is the neutrino energy, T, M_N, and $F(q^2)$ are the nuclear recoil energy, mass, and form factor, respectively, and

$$Q_w = Z g_p^V + N g_n^V, \tag{3}$$

is the weak nuclear charge, with Z, N the proton and neutron numbers of the detector material, and $g_p^V = 1/2 - 2\sin^2\theta_W$, $g_n^V = -1/2$. The nuclear form factor is approximately equal to 1 given the low energies of reactor antineutrinos. The number of events is calculated by convoluting the cross section with the reactor antineutrino spectra. The theoretical prediction of the Huber + Mueller model [36,37], with a 2.4% uncertainty, is considered. The uncertainties in the form factors are negligible with respect to the uncertainty in the antineutrino spectra [38].

A fit with the following χ^2 function is performed:

$$\chi^2 = \min_{\alpha,\beta,\gamma}\left[\left(\frac{N_{\text{meas}} - (1+\alpha)N_{\text{th}}(X,\gamma) - (1+\beta)B}{\sigma_{\text{stat}}}\right)^2 + \left(\frac{\alpha}{\sigma_\alpha}\right)^2 + \left(\frac{\beta}{\sigma_\beta}\right)^2 + \left(\frac{\gamma}{\sigma_\gamma}\right)^2\right], \tag{4}$$

where N_{meas} is the measured events, $N_{\text{th}}(X,\gamma)$ is the theoretical prediction with a threshold set at $(1+\gamma)100$ eV, B is the background coming from the reactor, σ_{stat} is the statistical uncertainty, and $\sigma_{\alpha,\beta,\gamma}$ are the systematic uncertainties on the signal, background, and energy threshold, respectively. The variable X refers to the parameter to be fitted. The statistical uncertainty can be expressed as

$$\sigma_{\text{stat}} = \sqrt{N_{\text{meas}} + B_{\text{cosm}}}, \tag{5}$$

where B_{cosm} is the background from cosmogenic neutrons.

The χ^2 function is minimized over the nuisance parameters α, β, and γ. Note that α is used to take into account the systematic errors coming from the antineutrino flux. The uncertainty of 2.4% from the Huber + Mueller model is translated to $\sigma_\alpha = 0.024$. On the other hand, β will consider the systematic error due to reactor backgrounds, which for the setup at the ININ is taken as 10%, namely $\sigma_\beta = 0.10$. This parameter is not included for setups B and B(1.5) since the location where the chamber would be placed at LV (30 m from the reactor core) is outside of the reactor building. Lastly, γ considers the uncertainty in the energy threshold, with an assumed value of 5% for setups A and B, based on previous experience calibrating the PICO bubble chambers. In addition, an uncertainty of 2% is assumed for setup B(1.5) to explore the maximum potential of this detector. The analysis performed is not sensitive to the energy threshold and reactor background uncertainties since the constraints are limited by the antineutrino flux uncertainty, due to the high number of events expected in one year for the three setups considered. All the uncertainties considered for the different setups are shown in Table I.

The following sections describe the new physics reach of the detector to a light scalar mediator, a sterile neutrino search, unitarity violation, and nonstandard interactions.

IV. LIGHT SCALAR MEDIATOR

A light scalar mediator with universal coupling to quarks and leptons is considered. In such a case, the effective dimension six operator is proportional to the square of the ratio of the coupling over the mass. The scalar contribution to the CEνNS cross section is expressed as

$$\frac{d\sigma}{dT} = \frac{M_N^2}{4\pi} \frac{g_\phi^4 Q_\phi^2 T}{E_\nu^2 (2M_N T + M_\phi^2)^2}, \tag{6}$$

which is added to the SM contribution without interference. Here, the coupling Q_ϕ is a function of the hadronic form factors $f_{T_q}^{p,n}$ [39]. The 95% exclusion regions for setups

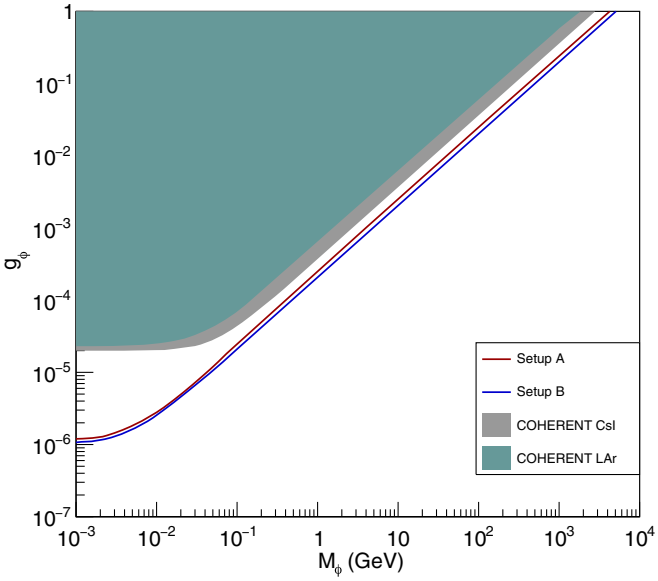

FIG. 1. Exclusion regions at 95% CL in the $g_\phi - M_\phi$ plane. The solid purple line represents the limit for setup A, while the orange line is the limit for setup B. The shaded brown and yellow regions correspond to the exclusions set by the COHERENT collaboration, using CsI [13] and LAr [14,40] detectors, respectively. These limits were calculated from data published by the COHERENT collaboration.

A and B in the plane $g_\phi - M_\phi$ are shown in Fig. 1, together with the current limits obtained using data from the COHERENT-CsI and -LAr measurements. The setups A and B will give stronger constraints than the current COHERENT data, due to the higher number of events expected.

V. STERILE NEUTRINO SEARCH

The three neutrino oscillations have been confirmed by many experiments [41–43] in agreement with the SM with three massive neutrinos. Despite this successful description, there are several experimental results [44–46] that could extend the current three flavor model, pointing to the existence of at least one additional sterile neutrino. These extra neutrinos are known as "sterile" since they might interact only through the mixing with the active states. CEνNS offers a window to search for sterile neutrinos, allowing to set constraints in different scenarios. A $3+1$ neutrino hypothesis is explored in this work, and sensitivity limits are established by measuring CEνNS with the scintillating bubble chamber near a reactor for the three setups under study. The $\bar{\nu}_e$ survival probability can be expressed as a function of the propagation length (L), the neutrino energy (E_ν), and the 4×4 neutrino mixing matrix as follows:

$$P_{\bar{\nu}_e\to\bar{\nu}_e}\left(\frac{L}{E_\nu}\right) = 1 - 4\sum_{k>j}|U_{ek}|^2|U_{ej}|^2\sin^2\left(\frac{\Delta m^2_{kj}L}{4E_\nu}\right),$$
$$= 1 - \sin^2 2\theta_{13}\sin^2\Delta_{13} - \sin^2 2\theta_{14}\sin^2\Delta_{41}, \quad (7)$$

where $U_{\alpha i}$ is the neutrino mixing matrix element for flavor ν_α ($\alpha = e, \mu, \tau$) and mass eigenstate ν_i ($i = 1, 2, 3$). The neutrino squared-mass differences are represented as $\Delta m^2_{ij} = m^2_i - m^2_j$, and Δ_{ij} is a function of the ratio L/E_ν, expressed as follows:

$$\Delta_{ij} = 1.267\Delta m^2_{ij}\left(\frac{L}{E_\nu}\right). \quad (8)$$

Figure 2 shows the limits established by individual analysis for the three setups and an analysis using the far/near ratio for setup A. This is possible due to the fact that the reactor considered for setup A is movable, inside a water pool. This results in baselines from 3 to 10 m. The far location considered is at 7 m, with the near at 3 m.

Setup B(1.5) will cover all the reactor anomaly, and it will give stronger constraints than any other experiment for $10 < |\Delta m^2_{41}| < 80$ eV^2. KARMEN + LSND [47] alternate the best limits with setup B(1.5) in the region $3 < |\Delta m^2_{41}| < 10$ eV^2. These results reflect the importance of reducing the uncertainty in the antineutrino flux since that is the only difference between setups B and B(1.5).

VI. UNITARITY VIOLATION

Measuring CEνNS in a reactor allows one to study unitarity violation (UV) in the neutrino mixing matrix, predicted by many new physics scenarios [48–51], including heavy sterile neutrinos. In this scenario, constraints are set in the nonunitarity parameters through the neutral current. The addition of extra heavy fermions implies the nonunitarity of the 3×3 light neutrino mixing matrix. In this case, the generalized charged current weak interaction mixing matrix is expressed as

$$N = N^{\mathrm{UV}}\cdot U^{3\times 3}, \quad (9)$$

where N^{UV} represents the UV effects corresponding to new physics, and $U^{3\times 3}$ is the standard 3×3 unitary mixing matrix [52]. The N^{UV} matrix can be parametrized as follows:

$$N^{\mathrm{UV}} = \begin{pmatrix} \alpha_{11} & 0 & 0 \\ \alpha_{21} & \alpha_{22} & 0 \\ \alpha_{31} & \alpha_{32} & \alpha_{33} \end{pmatrix}, \quad (10)$$

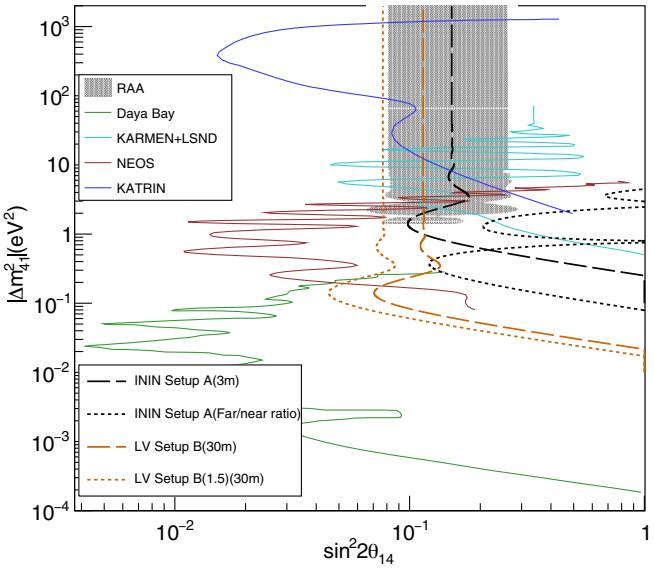

FIG. 2. Expected 95% CL exclusion region from sterile neutrino searches. The black dashed and dotted lines represent an expected limit for setup A with a distance of 3 m and for a far/near ratio, respectively. The far(near) location is at 7(3) m. The orange dashed and dotted lines characterize an exclusion sensitivity for setups B and B(1.5), respectively. A comparison of the sensitivity limits is performed with other experiments such as Daya Bay [54] 95% CL (green), KARMEN + LSND [47] 95% CL (light blue), NEOS [55] 90% CL (red), and KATRIN [56] 95% C.L (dark blue). The shaded region is allowed by the reactor antineutrino anomaly fit [55,57], enclosing favored solutions. The rest of the contours disfavor solutions to their right.

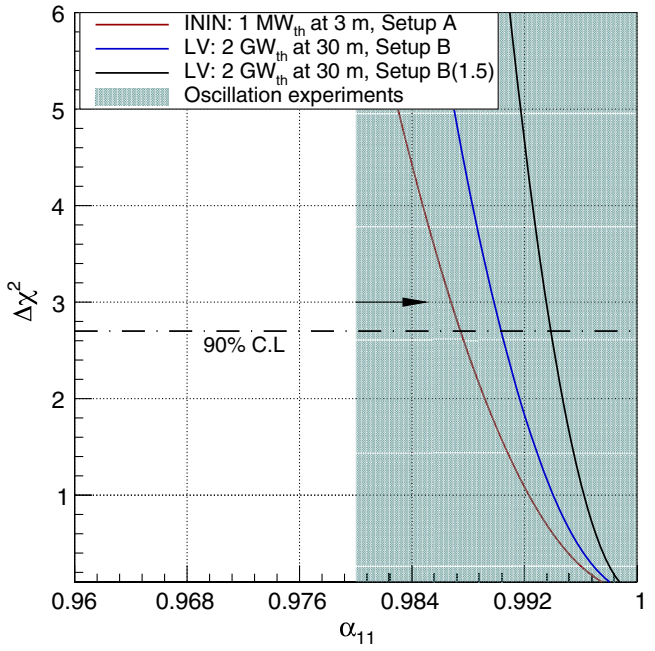

FIG. 3. Sensitivity of the diagonal parameter α_{11} for setups A (red), B (blue), and B(1.5) (black). The sensitivity from oscillation data [48] is also presented (blue shaded region). The fit was done by varying α_{11}, while α_{21} and α_{31} were marginalized. The three setups considered set better constraints, at 90% CL, than those obtained from oscillation data. Values are excluded to the left of the blue shaded region.

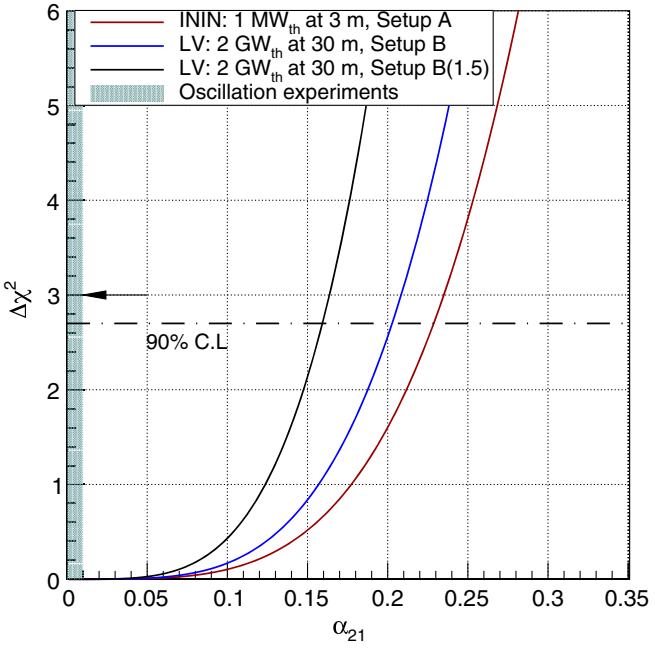

FIG. 4. Sensitivity of the nondiagonal parameter α_{21}. The projections for setups A (red), B (blue), and B(1.5) (black) are compared with upper limits from global oscillation fits [48] (blue shaded region). In this case, α_{21} was varied, while α_{11} and α_{31} were minimized. The oscillation data set better constraints at 90% CL Values are excluded to the right of the blue shaded region.

where the diagonal elements are real numbers and the off diagonal are complex. For the case of short-baseline experiments, such as the three setups considered in this work, the UV contribution arises from the zero-distance effect. Hence, the survival and transition probabilities of interest considering an electron antineutrino source can be expressed as

$$\begin{aligned} P_{ee} &= \alpha_{11}^4, \\ P_{e\mu} &= \alpha_{11}^2|\alpha_{21}|^2, \\ P_{e\tau} &= \alpha_{11}^2|\alpha_{31}|^2. \end{aligned} \tag{11}$$

The parameters α_{11}, α_{21}, and α_{31} are estimated with an χ^2 function identifying the optimal values of the parameters for setups A, B, and B(1.5). Since CEνNS is flavor blind, namely all the neutrino flavors are detected, $N_{\rm th}$ is given by the sum of the UV contributions of the three flavors as

$$N_{\rm th} = \alpha_{11}^2(\alpha_{11}^2 + |\alpha_{21}|^2 + |\alpha_{31}|^2)N_{\rm meas}, \tag{12}$$

where the fit for the χ^2 function is defined in Eq. (4).

Figures 3 and 4 show the expected sensitivities of the considered setups, to the diagonal and nondiagonal parameters, respectively, along with the current limits set by global neutrino oscillation data fits [53]. In addition, Fig. 5 presents the expected constraints [90% confidence level

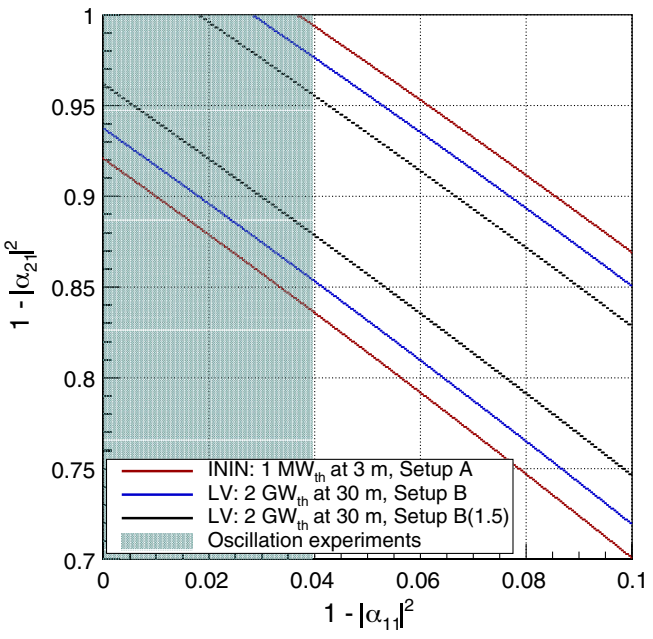

FIG. 5. Constraints at 90% CL on the deviations from unitarity in the $|\alpha_{21}|^2 - |\alpha_{11}|^2$ parameter space. Red, blue, and black lines correspond to setups A, B, and B(1.5), respectively. The sensitivity from oscillation experiments [48] is also presented (blue shaded region). In this analysis, α_{11} and α_{21} were varied, minimizing α_{31}. Values outside of the band delimited by the two lines are excluded.

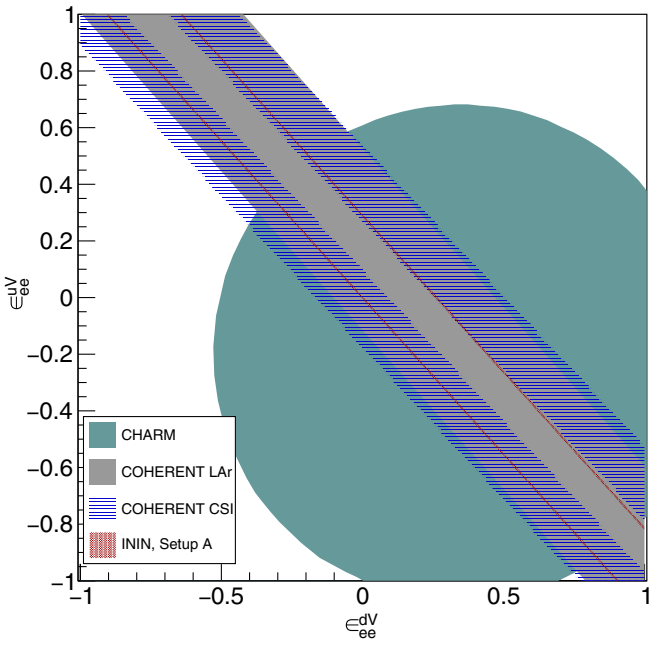

FIG. 6. Predicted sensitivity (90% CL) for setup A, represented as two red narrow bands, for parameters ε_{ee}^{fV} due to nonstandard interactions. Limits established by setups B and B(1.5) cover nearly an identical space parameter and are not shown. Allowed parameters established by the CHARM experiment (green) [58] and by the COHERENT experiment using LAr (blue) and CsI (grey) detectors [59] are also shown.

(CL)] in the $|\alpha_{21}|^2 - |\alpha_{11}|^2$ parameter space. It can be noted that the scintillating bubble chamber could establish stronger constraints than oscillation experiments for the case of α_{11}.

VII. NONSTANDARD INTERACTIONS

Any deviation from the SM CEνNS cross section would hint for physics beyond the Standard Model. The most common modification of the SM Lagrangian is through the nonstandard interactions (NSI) formalism, that consists of modifying the neutral current component with the extra contribution,

$$\mathcal{L}_{\mathrm{NC}}^{\mathrm{NSI}} = -2\sqrt{2}G_F \sum_{f,P,\alpha,\beta} \varepsilon_{\alpha\beta}^{fP}(\bar{\nu}_\alpha \gamma^\mu P_L \nu_\beta)(\bar{f}\gamma_\mu P_X f), \quad (13)$$

where f represents the u and d quarks, α and β correspond to the neutrino flavors (e, μ, τ), P_X is the right and left chirality projectors, and $\varepsilon_{\alpha\beta}^{fP}$ represents couplings that characterize the strength of the NSI. Figure 6 presents constraints (90% CL) to the values of the parameters ε_{ee}^{fV} from the projection of setup A. The constraints from COHERENT-LAr are the single gray band, while the COHERENT-CsI limits result in the two light-blue striped bands. Setup A is shown, which is the less restrictive setup for the scintillating bubble chamber. For this scenario, the constraints are no longer one band but two very narrow bands, shown in red color.

VIII. CONCLUSIONS

The sensitivity for different new physics scenarios of a low threshold LAr scintillating bubble chamber measuring CEνNS in a reactor has been investigated. The work reported in this manuscript shows better sensitivity than the current results established by the COHERENT collaboration, demonstrating the high potential of the bubble chamber technology. Searches for a light scalar mediator can achieve coupling values as low as $\sim 10^{-6}$ for masses of $\sim 10^{-3}$ GeV. By combining the setups described in the manuscript, namely a 10 kg detector at 3 m from a 1 MW_{th} reactor and a 100 kg detector at 30 m from a 2000 MW_{th} power reactor, a search for sterile neutrinos in the $|\Delta m_{41}^2|$ range of 10^{-2}–10^3 eV^2 would exclude the majority of the parameter space allowed by the reactor antineutrino anomaly. In addition, strong limits on the nonunitarity of the 3×3 neutrino mixing matrix are achieved after one year of exposure, competitive with current neutrino oscillation data fits. Lastly, results on nonstandard interactions by modifying the neutral current component with the addition of new couplings show complementarity with the results from the CHARM experiment. CEνNS experiments and, in particular, the scintillating bubble chamber, will be competitive to many diverse new physics scenarios. The scintillating bubble chamber detector could achieve a competitive and comprehensive physics program with setups in either research reactors or power commercial reactors.

ACKNOWLEDGMENTS

The authors would like to thank the SBC collaboration for useful discussions and for providing details of the Scintillating Bubble Chamber detector. This work is supported by the German-Mexican research collaboration Grants No. SP 778/4-1 (DFG) and No. 278017 (CONACYT), the Projects No. CONACYT CB-2017-2018/A1-S-13051 and No. CB-2017-2018/A1-S-8960, DGAPA UNAM Grants No. PAPIIT-IN107621, No. PAPIIT-IN107118 and No. PAPIIT-IN108020, and Fundación Marcos Moshinsky.

[1] G. Fernandez-Moroni, P. A. N. Machado, I. Martinez-Soler, Y. F. Perez-Gonzalez, D. Rodrigues, and S. Rosauro-Alcaraz, J. High Energy Phys. 03 (2021) 186.
[2] P. Coloma, I. Esteban, M. C. Gonzalez-Garcia, and J. Menendez, J. High Energy Phys. 08 (2020) 030.
[3] O. G. Miranda, D. K. Papoulias, G. Sanchez Garcia, O. Sanders, M. Tórtola, and J. W. F. Valle, J. High Energy Phys. 05 (2020) 130; 01 (2021) 067(E).
[4] M. Cadeddu, N. Cargioli, F. Dordei, C. Giunti, Y. F. Li, E. Picciau, C. A. Ternes, and Y. Y. Zhang, Phys. Rev. C **104**, 065502 (2021).
[5] D. K. Papoulias, T. S. Kosmas, and Y. Kuno, Front. Phys. **7**, 191 (2019).
[6] D. Aristizabal Sierra, V. De Romeri, and N. Rojas, J. High Energy Phys. 09 (2019) 069.
[7] M. F. Mustamin and M. Demirci, Braz. J. Phys. **51**, 813 (2021).
[8] O. G. Miranda, D. K. Papoulias, O. Sanders, M. Tórtola, and J. W. F. Valle, J. High Energy Phys. 12 (2021) 191.
[9] D. Aristizabal Sierra, V. De Romeri, L. J. Flores, and D. K. Papoulias, J. Cosmol. Astropart. Phys. 01 (2022) 055.
[10] A. Dasgupta, S. K. Kang, and J. E. Kim, J. High Energy Phys. 11 (2021) 120.
[11] J. Colaresi, J. I. Collar, T. W. Hossbach, A. R. L. Kavner, C. M. Lewis, A. E. Robinson, and K. M. Yocum, Phys. Rev. D **104**, 072003 (2021).
[12] O. G. Miranda, D. K. Papoulias, G. Sanchez Garcia, O. Sanders, M. Tórtola, and J. W. F. Valle, J. Phys. Conf. Ser. **2156**, 012132 (2021).
[13] D. Akimov *et al.* (COHERENT Collaboration), Science **357**, 1123 (2017).
[14] D. Akimov *et al.* (COHERENT Collaboration), Phys. Rev. Lett. **126**, 012002 (2021).
[15] A. Aguilar-Arevalo *et al.* (CONNIE Collaboration), Phys. Rev. D **100**, 092005 (2019).
[16] H. Bonet *et al.* (CONUS Collaboration), Phys. Rev. Lett. **126**, 041804 (2021).
[17] V. Belov *et al.*, J. Instrum. **10**, P12011 (2015).
[18] G. Agnolet *et al.* (MINER COLLABORATION), Nucl. Instrum. Methods Phys. Res., Sect. A **853**, 53 (2017).
[19] R. Strauss *et al.*, Eur. Phys. J. C **77**, 506 (2017).
[20] J. Billard, J. Johnston, and B. J. Kavanagh, J. Cosmol. Astropart. Phys. 11 (2018) 016.
[21] D. Akimov *et al.*, J. Instrum. **12**, C06018 (2017).
[22] Y. Abreu *et al.* (SoLid Collaboration), J. Instrum. **16**, P02025 (2021).
[23] J. Colaresi, J. I. Collar, T. W. Hossbach, C. M. Lewis, and K. M. Yocum, arXiv:2202.09672.
[24] I. Alekseev *et al.* (nuGeN Collaboration), arXiv:2205.04305.
[25] P. Giampa (SBC Collaboration), Proc. Sci. ICHEP2020 (**2021**) 632.
[26] L. J. Flores *et al.* (CEνNS Theory Group at IF-UNAM and SBC Collaboration), Phys. Rev. D **103**, L091301 (2021).
[27] D. Baxter *et al.*, Phys. Rev. Lett. **118**, 231301 (2017).
[28] J. Berset, M. Burns, G. Harigel, J. Lindsay, G. Linser, and F. Schenk, Nucl. Instrum. Methods Phys. Res. **203**, 141 (1982).
[29] G. Harigel, H. Hilke, G. Linser, and F. Schenk, Nucl. Instrum. Methods Phys. Res. **188**, 517 (1981).
[30] D. Durnford and M.-C. Piro (SBC and PICO Collaborations), J. Instrum. **17**, C01030 (2022).
[31] B. Ali *et al.* (PICO Collaborations), arXiv:2205.05771.
[32] D. Adey *et al.* (Daya Bay Collaborations), Phys. Rev. D **100**, 052004 (2019).
[33] S. Agostinelli *et al.* (GEANT4 Collaborations), Nucl. Instrum. Methods Phys. Res., Sect. A **506**, 250 (2003).
[34] J. Allison *et al.*, IEEE Trans. Nucl. Sci. **53**, 270 (2006).
[35] J. Allison *et al.*, Nucl. Instrum. Methods Phys. Res., Sect. A **835**, 186 (2016).
[36] P. Huber, Phys. Rev. C **84**, 024617 (2011); **85**, 029901(E) (2012).
[37] T. Mueller *et al.*, Phys. Rev. C **83**, 054615 (2011).
[38] O. Tomalak, P. Machado, V. Pandey, and R. Plestid, J. High Energy Phys. 02 (2021) 097.
[39] M. Hoferichter, J. Ruiz de Elvira, B. Kubis, and U.-G. Meißner, Phys. Rev. Lett. **115**, 092301 (2015).
[40] D. Akimov *et al.* (COHERENT Collaborations), 10.5281/zenodo.3903810 (2020).
[41] Y. Fukuda *et al.* (Super-Kamiokande Collaborations), Phys. Rev. Lett. **81**, 1562 (1998).
[42] Q. R. Ahmad *et al.* (SNO Collaborations), Phys. Rev. Lett. **89**, 011301 (2002).
[43] K. Eguchi *et al.* (KamLAND Collaborations), Phys. Rev. Lett. **90**, 021802 (2003).
[44] C. Athanassopoulos *et al.* (LSND Collaborations), Phys. Rev. Lett. **77**, 3082 (1996).
[45] J. N. Abdurashitov *et al.* (SAGE Collaborations), Phys. Rev. C **80**, 015807 (2009).
[46] A. A. Aguilar-Arevalo *et al.* (MiniBooNE Collaborations), Phys. Rev. Lett. **110**, 161801 (2013).
[47] J. M. Conrad and M. H. Shaevitz, Phys. Rev. D **85**, 013017 (2012).
[48] O. G. Miranda, D. K. Papoulias, O. Sanders, M. Tórtola, and J. W. F. Valle, Phys. Rev. D **102**, 113014 (2020).
[49] C. Soumya, Phys. Rev. D **105**, 015012 (2022).
[50] D. V. Forero, C. Giunti, C. A. Ternes, and M. Tortola, Phys. Rev. D **104**, 075030 (2021).
[51] Y. Wang and S. Zhou, Phys. Lett. B **824**, 136797 (2022).
[52] W. Rodejohann and J. W. F. Valle, Phys. Rev. D **84**, 073011 (2011).
[53] F. J. Escrihuela, D. V. Forero, O. G. Miranda, M. Tórtola, and J. W. F. Valle, New J. Phys. **19**, 093005 (2017).
[54] F. P. An *et al.* (Daya Bay Collaborations), Phys. Rev. Lett. **117**, 151802 (2016).
[55] Y. J. Ko *et al.* (NEOS Collaborations), Phys. Rev. Lett. **118**, 121802 (2017).
[56] M. Aker *et al.* (KATRIN Collaborations), Phys. Rev. Lett. **126**, 091803 (2021).
[57] G. Mention, M. Fechner, T. Lasserre, T. A. Mueller, D. Lhuillier, M. Cribier, and A. Letourneau, Phys. Rev. D **83**, 073006 (2011).
[58] J. Dorenbosch *et al.* (CHARM Collaborations), Phys. Lett. B **180**, 303 (1986).
[59] D. Akimov *et al.* (COHERENT Collaborations), Phys. Rev. D **100**, 115020 (2019).